

Linear viscoelasticity of a dilute active suspension

Toni M. Bechtel¹ · Aditya S. Khair¹

Received: 20 September 2016 / Revised: 10 December 2016 / Accepted: 18 December 2016 / Published online: 7 January 2017
© Springer-Verlag Berlin Heidelberg 2017

Abstract The linear viscoelasticity of a dilute suspension of active (self-propelled) rigid spheroidal particles is calculated under a small-amplitude oscillatory shear (SAOS) deformation. The imposed shear acts to drive the microstructure of the suspension, as parameterized by the orientational probability distribution function, out of equilibrium. The microstructure relaxes via two independent mechanisms: rotational Brownian motion and correlated tumbling; the combination of which results in an increased rate of stress relaxation, relative to a suspension that relaxes solely by either mechanism. We explicitly calculate the non-equilibrium orientational microstructure due to the SAOS deformation, rotational diffusion, and tumbling. From this, we determine the linear viscoelasticity of the suspension from the orientationally averaged stresslet, which arises from the imposed flow, rotational diffusion, and particle activity (self-propulsion). Next, we demonstrate that a modified Cox-Merz rule is applicable to a dilute, active suspension via a comparison of our linear viscoelasticity results to a theoretical prediction of the steady shear viscosity of active, slender rods (Saintillan, *Exp Mech* 50(9) 1275–1281, 2010). Finally, through a comparison of our results to experiments on *Escherichia coli* (López et al., *Phys Rev Lett* 115(2) 028, 301, 2015), we show that the linear viscoelasticity of an active suspension can be utilized to determine the mechanism of self-propulsion (i.e., pusher or puller),

and estimate the strength of self-propulsion and correlation between tumbling events.

Keywords Active suspension · Microstructure · Linear viscoelasticity · Cox-Merz rule

Introduction

Recently, there has been an intense interest in the dynamics of active, self-propelled particles, such as biological micro-organisms and synthetic colloidal motors (Ebbens and Howse 2010; Hong et al. 2010; Patra et al. 2013; Dey et al. 2016; Schwarz-Linek et al. 2016; Teo and Pumerá 2016). Self-propelled particles have potential biomedical applications, including targeted drug delivery (Kline et al. 2005; Dhar et al. 2007; Sundararajan et al. 2008), where a drug is transported in or on an active particle through the bloodstream directly to a predetermined location, e.g., a cancerous tumor or region of inflammation. Furthermore, suspensions of self-propelled microscale particles serve as a paradigmatic model for active matter, which is inherently out of thermal equilibrium due to the activity of the particles (Tjhung et al. 2011; Stenhammar et al. 2014; Takatori et al. 2014; Spagnolie 2015). A natural question that arises is as follows: How does the activity of the particles impact the rheology, or state of the stress, in a flowing suspension? For example, how would the addition of active particles, for use in drug delivery, impact the rheology and subsequent blood flow in a patient? Conversely, what can the stress of an active suspension tell us about the activity (e.g., mechanism or strength of self-propulsion) of the particles in suspension?

✉ Aditya S. Khair
akhair@andrew.cmu.edu

¹ Department of Chemical Engineering, Carnegie Mellon University, Pittsburgh, PA 15213, USA

In general, microscale self-propelled particles, at low Reynolds number, can be divided into two categories: pullers and pushers. Pullers, such as *Chlamydomonas reinhardtii* (CR), generate thrust from the front of their body; whereas, pushers, such as *Escherichia coli* (*E. coli*) or *Bacillus subtilis* (*B. subtilis*), generate thrust from their rear (Lauga and Powers 2009). Steady shear experiments on a dilute suspension of CR have shown that the effective viscosity of the suspension is increased, relative to both the viscosity of the suspending medium and the viscosity of a suspension of the same immotile (i.e., dead) bacteria (Rafai et al. 2010; Mussler et al. 2013). Experiments conducted on dilute suspensions of pushers, *E. coli* (Gachelin et al. 2013; López et al. 2015) and *B. subtilis* (Sokolov and Aranson 2009), reported a steady shear viscosity less than that of a suspension of the same immotile bacteria and, more surprisingly, also less than the steady shear viscosity of the suspending medium. This indicates a negative particle contribution to the overall suspension viscosity.

From these experimental results, it is evident that the activity of the particles affects the stress in the suspension. The activity of the particles has an indirect effect on the stress by altering the microstructure, or spatio-temporal arrangement, of the suspension through tumbling, which acts to randomize the particle orientation, as observed in *E. coli* (Turner et al. 2000). The activity of the particles also has a direct effect on the stress via the force dipole (stresslet) generated from self-propulsion (Saintillan 2010; Takatori et al. 2014; Spagnolie 2015). One methodology to predict the stress of an active suspension is to calculate the disturbance flow created by the active particles. Then, from the energy dissipation associated with this, the effective viscosity can be inferred. Haines et al. (2008) utilized a two-dimensional hydrodynamics simulation to calculate the disturbance flow, and hence rheology, of a dilute, active suspension of disks. Hatwalne et al. (2004) utilized a coarse-grained model based on the field theory of nematic liquid crystals to predict the linear viscoelasticity of a dilute suspension of active disks or rods. Alternatively, one can explicitly determine how the activity of the particles affects the microstructure of the suspension and from there predict the microstructurally averaged stress. In this vein, Saintillan (2010) utilized a kinetic theory model to calculate the change in the orientational microstructure of a dilute suspension of active, slender rods, resulting from an imposed steady shear flow, rotational Brownian motion, and uncorrelated tumbling events (i.e., 90° changes in orientation due to tumbling). Bozorgi and Underhill (2014) calculated the stress in a dilute suspension of slender, active rods subject to a large-amplitude oscillatory shear (LAOS) deformation. They assumed that the tumbling events did not affect the microstructure of the suspension, but did include the direct stress contribution arising from the particle activity.

In this work, we calculate the linear viscoelasticity of a dilute suspension of active, spheroidal particles, of arbitrary aspect ratio, subject to a small-amplitude oscillatory shear (SAOS) deformation. We explicitly account for microstructural relaxation due to both rotational Brownian motion and correlated tumbling, as this is relevant for many biological systems. For instance, *E. coli* are Brownian, prolate bodies with an average change in orientation due to tumbling of $58 \pm 40^\circ$ (Turner et al. 2000). Oscillatory shear experiments are useful in that they allow for one to average the measured signal over multiple oscillation cycles and avoid step changes that occur during the start-up and cessation of a steady flow. SAOS experiments effectively allow one to take a spectral fingerprint of the linear response of a material. The frequency-dependent results obtained from a SAOS deformation can be used to predict steady shear behavior via the empirical Cox-Merz rule, which states that the magnitude of the frequency-dependent complex viscosity is equivalent to steady shear viscosity (Cox and Merz 1958). Thus, information from a SAOS deformation can be utilized to predict the steady shear viscosity of a material, which is advantageous as it is typically simpler to experimentally perform a frequency-sweep as opposed to a shear rate sweep (Macosko 1994). This could be especially true for active suspensions of biological organisms, where large shear rates could be detrimental to the organisms and inhibit activity. Gachelin et al. (2013) observed that the effective steady shear viscosity of both a motile and immotile dilute suspension of *E. coli* were equivalent at high shear rates, indicating that the active contribution to the steady shear viscosity is negligible compared to the passive contribution in this regime. There are cases where the Cox-Merz rule breaks down, namely colloidal dispersions at high shear rate and frequency (Al-Hadithi et al. 1992), and thus, it should be viewed as a “rule-of-thumb” rather than a strict rule.

For a homogeneous, oscillatory shear deformation, the strain-rate is given by $\dot{\gamma} = \dot{\gamma}_0 \cos(\omega t)$, where $\dot{\gamma}_0$ is the strain-rate amplitude and ω is the oscillation frequency. Two timescales arise: (1) the oscillation timescale, $1/\omega$ and (2) the flow timescale, $1/\dot{\gamma}_0$. The active suspension is also characterized by two independent relaxation mechanisms: Brownian rotation and tumbling. Therefore, we can form two ratios of the flow to relaxation timescales, or Weissenberg numbers: $Wi_D = \dot{\gamma}_0/D_r$ and $Wi = \dot{\gamma}_0/\tau^{-1}$, where D_r is the rotary diffusion coefficient and τ^{-1} is frequency of tumbling. Furthermore, a relative rate of relaxation can be defined as $\lambda = Wi/Wi_D = D_r/\tau^{-1}$. For a dilute suspension of *E. coli*, $\lambda \sim 0.1$ (using $D_r \sim 0.1 \text{ s}^{-1}$ and $\tau^{-1} \sim 1 \text{ s}^{-1}$ (Leal and Hinch 1971; Gachelin et al. 2013)) and tumbling is therefore the dominant mode of microstructural relaxation. SAOS requires that the rate of relaxation is much greater than the rate of deformation, $Wi \ll 1$. Thus,

the linear viscoelasticity of a dilute suspension of active spheroids is examined in this regime.

In the “[Governing equations](#)” section, we detail the governing equations required to calculate the microstructure and linear viscoelasticity of the active suspension. In the “[Asymptotic expansion for linear viscoelasticity](#)” section, a solution for the microstructure is obtained via an asymptotic analysis for $Wi \ll 1$. In the “[Linear viscoelasticity](#)” section, the deviatoric particle contribution to the suspension stress is calculated, and the combined effects of the imposed flow, Brownian rotation, and tumbling are discussed. Finally, in the “[Comparison to previous work](#)” section, we demonstrate that a Cox-Merz rule can be applied to an active particle suspension by comparing our linear viscoelastic results to (1) a theoretical prediction of the steady shear viscosity of active, slender rods (Saintillan 2010) and (2) experimental data for the steady shear viscosity of a dilute suspension of *E. coli* (López et al. 2015). We also demonstrate that from the linear viscoelasticity one can determine the method of self-propulsion (pusher or puller) and estimate the strength of self-propulsion and correlation between tumbling events.

Governing equations

A suspension of active particles is modeled as an ensemble of Brownian, rigid spheroids in a Newtonian fluid of viscosity μ_s and density ρ . The particles are assumed to be free of any externally applied force or torque and are characterized by an aspect ratio, r , defined as the ratio of the major (ℓ) to minor (a) axes, $r = \ell/a$. The hydrodynamic sphericity of the particles is given by the Bretherton constant,

$$B = \frac{r^2 - 1}{r^2 + 1}, \tag{1}$$

which is negative for oblate spheroids, positive for prolate spheroids, and zero for spheres. The suspension is assumed to be dilute, such that interparticle interactions can be neglected. Thus, $c = 4\pi n\ell a^2/3 \ll 1$, where c is the particle volume fraction and n is the number density. We will consider an oscillatory shear flow with velocity field $\mathbf{v} = \dot{\gamma}_0 y \cos(\alpha \tilde{t}) \mathbf{e}_x$, and velocity gradient $\nabla \mathbf{v} = \dot{\gamma}_0 \cos(\alpha \tilde{t}) \mathbf{e}_y \mathbf{e}_x$, where $\mathbf{e}_x, \mathbf{e}_y, \mathbf{e}_z$ are Cartesian unit vectors in the flow, flow-gradient, and vorticity directions, respectively, α is the dimensionless oscillation frequency, and \tilde{t} is dimensionless time ($\alpha = \omega\tau, \tilde{t} = t/\tau$).

The microstructure of the suspension is characterized by the orientation distribution function, $\psi(\mathbf{p}, t)$, where $\psi(\mathbf{p}, t) \sin\theta d\theta d\phi$ represents the probability of finding a particle ensemble in a differential region about (θ, ϕ) (Hinch and Leal 1972; Kim and Karrila 2005). Here, \mathbf{p} is a

unit vector along the particle axis of symmetry, in spherical coordinates, and θ and ϕ are the polar and azimuthal angles, respectively. The orientation distribution function satisfies a conservation, or Fokker-Planck, equation (Subramanian and Koch 2009),

$$\frac{\partial \psi}{\partial t} + \nabla_{\mathbf{p}} \cdot (\dot{\mathbf{p}} \psi) = D_r \nabla_{\mathbf{p}}^2 \psi - \tau^{-1} \left(\psi - \int K(\mathbf{p}|\mathbf{p}') \psi(\mathbf{p}', \tilde{t}) dS' \right), \tag{2}$$

where $\nabla_{\mathbf{p}}$ is the surface gradient operator, and $\dot{\mathbf{p}}$ is the deterministic evolution of the particle orientation due to the ambient shear (Jeffery 1922; Brenner and Condiff 1974; Kim and Karrila 2005),

$$\dot{\mathbf{p}} = B(\mathbf{I} - \mathbf{p}\mathbf{p}) \cdot \mathbf{H} \cdot \mathbf{p}, \tag{3}$$

where \mathbf{I} is the identity tensor and $\mathbf{H} = B^{-1}\mathbf{\Omega} + \mathbf{E}$. Here, $\mathbf{\Omega}$ is the vorticity tensor and \mathbf{E} is the rate of strain tensor, such that $\nabla \mathbf{v} = \mathbf{E} + \mathbf{\Omega}$. For an oscillatory shear deformation, $\mathbf{H} = \dot{\gamma}_0 \cos(\alpha \tilde{t}) \check{\mathbf{H}}$, where,

$$\check{\mathbf{H}} = \frac{1}{2} \left[(1 - B^{-1}) \mathbf{e}_x \mathbf{e}_y + (1 + B^{-1}) \mathbf{e}_y \mathbf{e}_x \right]. \tag{4}$$

The first term on the right-hand-side (RHS) of Eq. 2 accounts for the randomization of particle orientation due to rotational Brownian diffusion. The last terms on the RHS, in parentheses, of Eq. 2 model the randomization of particle orientation due to tumbling events. Specifically, tumbling events are treated as a Poisson process (Subramanian and Koch 2009). Here, $K(\mathbf{p}|\mathbf{p}')$ is a conditional probability density function characterizing a tumble from orientation \mathbf{p}' to orientation \mathbf{p} , where the apostrophe indicates the pre-tumble orientation, and $dS' = \sin\theta' d\theta' d\phi'$ is the pre-tumble differential solid angle. Conservation of probability requires that,

$$\int K(\mathbf{p}|\mathbf{p}') dS = \int K(\mathbf{p}|\mathbf{p}') dS' = 1. \tag{5}$$

Following Subramanian and Koch (2009), we choose

$$K(\mathbf{p}|\mathbf{p}') = \frac{\beta}{4\pi \sinh \beta} \exp(\beta \mathbf{p} \cdot \mathbf{p}'), \tag{6}$$

where β is parameter that gauges the correlation between pre- and post-tumble configurations. In the limit of $\beta \rightarrow 0$, $K = 1/4\pi$, corresponding to uncorrelated tumbles (90° changes in orientation), and the term in parentheses on the RHS of Eq. 2 reduces to the relaxation-time approximation used in the kinetic theory of gases (Chapman and Cowling 1991; McQuarrie 2000). This limit was previously investigated by Saintillan (2010) for slender, active rods in steady shear. In the limit of $\beta \rightarrow \infty$, each tumbling event results in an infinitesimal change in orientation, and thus,

microstructural relaxation is dominated by rotational diffusion. This regime was investigated by Bozorgi and Underhill (2014). The inclusion of finite, non-zero values of β allows one to account for correlated tumbles. For instance, the average change in orientation due to tumbling ($\langle \theta \rangle$) for an *E. coli* cell is $58 \pm 40^\circ$ (Turner et al. 2000), which corresponds to $\beta \sim 1.5$, where (Subramanian and Koch 2009),

$$\langle \theta \rangle = \frac{\beta}{2 \sinh \beta} \int_0^\pi e^{\beta \cos \theta} \sin \theta d\theta. \tag{7}$$

A dimensionless conservation equation can be obtained by normalizing \mathbf{H} by the strain-rate amplitude ($\mathbf{H} = \dot{\gamma}_0 \tilde{\mathbf{H}}$). Substitution of Eq. 3 into Eq. 2 yields,

$$\frac{\partial \psi}{\partial \tilde{t}} + B Wi \nabla_{\mathbf{p}} \cdot [(\mathbf{I} - \mathbf{pp}) \cdot \tilde{\mathbf{H}} \cdot \mathbf{p} \psi] = \lambda \nabla_{\mathbf{p}}^2 \psi - \left(\psi - \int K(\mathbf{p}|\mathbf{p}') \psi(\mathbf{p}', \tilde{t}) dS' \right), \tag{8}$$

The orientation distribution function is also subject to a normalization condition, $\int \psi(\mathbf{p}, t) dS = 1$.

Asymptotic expansion for linear viscoelasticity

The conservation (8) is to be addressed in the limit of weak deformation rate, $Wi \ll 1$. In this regime, the microstructure remains in a near-equilibrium state, and the orientation distribution function can be expressed as a regular perturbation expansion,

$$\psi(\mathbf{p}, t) = \frac{1}{4\pi} \left(1 + Wi \psi_1(\mathbf{p}, t) + O(Wi^2) \right), \tag{9}$$

where $Wi \psi_1$ represents the leading order departure from equilibrium. Substitution of Eq. 9 into Eq. 8 yields,

$$\begin{aligned} \frac{\partial \psi_1}{\partial \tilde{t}} = & 3B \cos(\alpha \tilde{t}) \mathbf{pp} : \check{\mathbf{E}} \\ & + \lambda \left[(\mathbf{I} - \mathbf{pp}) : \frac{\partial^2 \psi_1}{\partial \mathbf{p} \partial \mathbf{p}} - 2\mathbf{p} \cdot \frac{\partial \psi_1}{\partial \mathbf{p}} \right] \\ & - \left(\psi_1 - \int K \psi_1(\mathbf{p}', \tilde{t}) dS' \right), \end{aligned} \tag{10}$$

subject to $\int \psi_1 dS = 0$. Here, $\mathbf{E} = \dot{\gamma}_0 \cos(\alpha \tilde{t}) \check{\mathbf{E}}$ and $\check{\mathbf{E}} = \frac{1}{2} (\mathbf{e}_x \mathbf{e}_y + \mathbf{e}_y \mathbf{e}_x)$. The solution to Eq. 10 should oscillate at the input frequency, α , and linearly depend on the imposed flow through the quadrupolar forcing $3B \cos(\alpha \tilde{t}) \mathbf{pp} : \check{\mathbf{E}}$, which acts to align the microstructure along the principle axes of strain. Hence, we pose,

$$\psi_1(\mathbf{p}, \tilde{t}) = \left(h_1 e^{i\alpha \tilde{t}} + \hat{h}_1 e^{-i\alpha \tilde{t}} \right) \mathbf{pp} : \check{\mathbf{E}}, \tag{11}$$

where hatted quantities indicate complex conjugates. Substitution of Eq. 11 into Eq. 10 yields an algebraic equation for h_1 , with solution,

$$h_1 = \frac{3B}{2} \left[\frac{1 - J(\beta) + 6\lambda - i\alpha}{\alpha^2 + (1 - J(\beta) + 6\lambda)^2} \right], \tag{12}$$

where $i = \sqrt{-1}$ and

$$J(\beta) = \frac{(3 + \beta^2) \sinh \beta - 3\beta \cosh \beta}{\beta^2 \sinh \beta}. \tag{13}$$

To determine (12) and (13), we have used the result: $\int K \mathbf{p}' \mathbf{p}' : \check{\mathbf{E}} dS' = J(\beta) \mathbf{pp} : \check{\mathbf{E}}$. A derivation of this relation can be found in Appendix B of Subramanian and Koch (2009); in their equation (B8), the coefficient of $\sinh \beta$ is incorrect and should read $-(3\beta^2 + 6)$. The expression in Eq. 13 is even and is bounded by $J(\beta) = [0, 1)$, corresponding to $\beta = [0, \pm\infty)$. Next, we utilize our asymptotic solution to the orientation distribution function to calculate the linear viscoelasticity of the suspension.

Linear viscoelasticity

The particle contribution to the deviatoric stress of the suspension ($\boldsymbol{\tau}^p$) is obtained from an ensemble average of the stresslet, which can be decomposed into three contributions arising from: the imposed flow ($\boldsymbol{\tau}^F$), rotational Brownian motion ($\boldsymbol{\tau}^B$), and the active nature (self-propulsion) of the particles ($\boldsymbol{\tau}^A$),

$$\boldsymbol{\tau}^p = \boldsymbol{\tau}^F + \boldsymbol{\tau}^B + \boldsymbol{\tau}^A. \tag{14}$$

The contribution from the imposed flow is given by Hinch and Leal (1976) and Kim and Karrila (2005),

$$\begin{aligned} \boldsymbol{\tau}^F = & 2\mu_s c \left[2A_H \left(\langle \mathbf{pppp} \rangle - \frac{1}{3} \langle \mathbf{pp} \rangle \right) : \mathbf{E} \right. \\ & + 2B_H \left(\mathbf{E} \cdot \langle \mathbf{pp} \rangle + \langle \mathbf{pp} \rangle \cdot \mathbf{E} \right. \\ & \left. \left. + \frac{2\mathbf{I}}{3} \mathbf{E} : \langle \mathbf{pp} \rangle \right) + C_H \mathbf{E} \right], \end{aligned} \tag{15}$$

where the angled brackets are orientational averages,

$$\langle \mathbf{pp} \rangle = \int \mathbf{pp} \psi(\mathbf{p}, \tilde{t}) dS, \tag{16}$$

and similarly for $\langle \mathbf{pppp} \rangle$. The torque generated from rotational Brownian motion leads to the following stress contribution (Hinch and Leal 1976; Kim and Karrila 2005),

$$\boldsymbol{\tau}^B = 2\mu_s c F_H D_r \left(\langle \mathbf{pp} \rangle - \frac{\mathbf{I}}{3} \right). \tag{17}$$

Here, $A_H, B_H, C_H,$ and F_H are known scalar functions of the particle aspect ratio, r , Hinch and Leal (1972) and Kim and Karrila (2005). Finally, the self-propulsion of the particles exerts a force dipole onto the fluid, resulting in the active stress contribution (Saintillan and Shelley 2008),

$$\boldsymbol{\tau}^A = n\sigma_0 \left(\langle \mathbf{pp} \rangle - \frac{\mathbf{I}}{3} \right), \tag{18}$$

where σ_0 is a scalar dipole strength, in units of energy. The sign of σ_0 indicates the mechanism of self-propulsion (i.e., $\sigma_0 < 0$ for pushers and $\sigma_0 > 0$ for pullers) and the magnitude of σ_0 scales with the swimming speed of the particle (Saintillan and Shelley 2008)

Substitution of Eqs. 11 and 12 into Eqs. 15, 17 and 18 yields for the shear component of the stress, τ_{yx} ,

$$\frac{\tau_{yx}^F}{\dot{\gamma}_0 \mu_s c} = \left(\frac{4A_H}{15} + \frac{2B_H}{3} + C_H \right) \cos(\alpha \tilde{t}) + O(Wi), \tag{19}$$

$$\begin{aligned} \frac{\tau_{yx}^B}{\dot{\gamma}_0 \mu_s c} = & \frac{2F_H B \lambda}{5} \left[\frac{1 - J(\beta) + 6\lambda}{\alpha^2 + (1 - J(\beta) + 6\lambda)^2} \cos(\alpha \tilde{t}) \right. \\ & \left. + \frac{\alpha}{\alpha^2 + (1 - J(\beta) + 6\lambda)^2} \sin(\alpha \tilde{t}) \right] + O(Wi), \end{aligned} \tag{20}$$

and

$$\begin{aligned} \frac{\tau_{yx}^A}{\dot{\gamma}_0 \mu_s c} = & \frac{zB}{5} \left[\frac{1 - J(\beta) + 6\lambda}{\alpha^2 + (1 - J(\beta) + 6\lambda)^2} \cos(\alpha \tilde{t}) \right. \\ & \left. + \frac{\alpha}{\alpha^2 + (1 - J(\beta) + 6\lambda)^2} \sin(\alpha \tilde{t}) \right] + O(Wi). \end{aligned} \tag{21}$$

Note that the shear component of the stress is all that is obtained from linear viscoelasticity; normal stress differences can be obtained at $O(Wi^2)$, requiring knowledge of ψ_2 . Here, $z = \sigma_0 \tau / \mu_s V_p$ is a dimensionless dipole moment and V_p is the volume of a single particle. For $\lambda < 1$ ($\lambda > 1$), the frequency of tumbling is greater (less) than the frequency of rotational Brownian motion; the dominant relaxation mechanism is tumbling (rotational Brownian motion). The overall particle contribution to the deviatoric stress can be expressed as the sum of a viscous and elastic response,

$$\frac{\tau_{yx}^p}{\dot{\gamma}_0} = \eta'(\alpha) \cos(\alpha \tilde{t}) + \eta''(\alpha) \sin(\alpha \tilde{t}) + O(Wi), \tag{22}$$

where η' and η'' are the viscous and elastic components of the complex viscosity ($\eta^* = \eta' + i\eta''$), respectively, which are given by,

$$\begin{aligned} \frac{\eta'}{\mu_s c} = & \frac{4A_H}{15} + \frac{2B_H}{3} + C_H \\ & + \frac{B}{5} (2F_H \lambda + z) \frac{1 - J(\beta) + 6\lambda}{\alpha^2 + (1 - J(\beta) + 6\lambda)^2}, \end{aligned} \tag{23}$$

and

$$\frac{\eta''}{\mu_s c} = \frac{B}{5} (2F_H \lambda + z) \frac{\alpha}{\alpha^2 + (1 - J(\beta) + 6\lambda)^2}. \tag{24}$$

Figure 1 shows the effect of correlated tumbling ($\beta \neq 0$) on the magnitude of the viscous and elastic components of the complex viscosity. Correlated tumbling events increase the magnitude of the Brownian and active stress response,

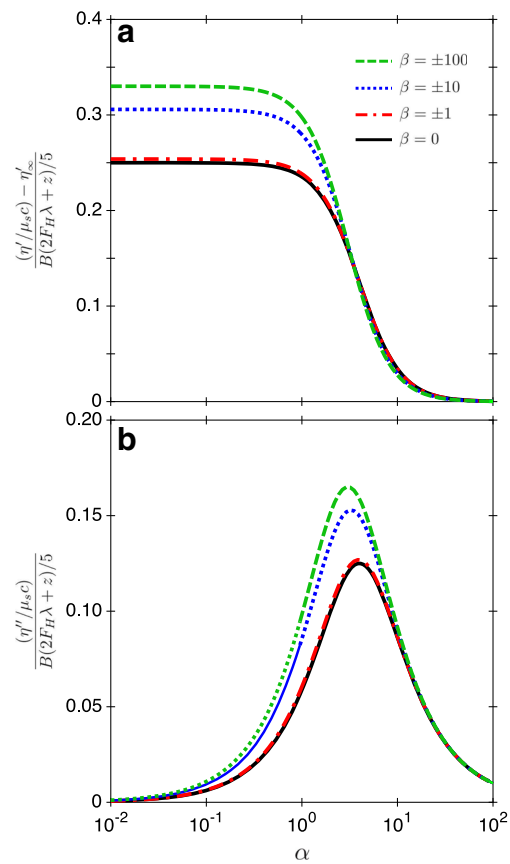


Fig. 1 Effect of correlated tumbling ($\beta \neq 0$) on **a** the viscous and **b** elastic components of the complex viscosity for $\lambda = 0.5$. Here, $\eta'_{\infty} = 4A_H/15 + 2B_H/3 + C_H$ is the viscous complex viscosity in the limit of $\alpha \rightarrow \infty$. Correlated tumbling events increase the magnitude of the Brownian and active stress contribution at small to moderate frequency values ($\alpha \lesssim 10$), resulting in an increased magnitude of the viscous and elastic components

compared to uncorrelated tumbling events, at small and moderate frequency values ($\alpha \leq O(10)$).

Since z can be positive or negative, depending on the mechanism of self-propulsion, we can define a critical dipole strength, z^* , at which the particle contribution to the zero-frequency viscous complex viscosity is zero ($\eta'(0) = 0$),

$$z^* = \frac{5}{B(1 - J(\beta) + 6\lambda)} \left(\frac{4A_H}{15} + \frac{2B_H}{3} + C_H \right) + 2F_H\lambda, \quad (25)$$

which is positive for prolate spheroids and negative for oblate spheroids, the latter since $B, F_H < 0$ for $r < 1$. Thus, a dispersion of prolate pushers with dipole strength $z < -z^*$ can have a negative contribution to the overall viscosity of the suspension, as previously predicted (Hatwalne et al. 2004; Haines et al. 2008; Saintillan 2010)

and observed (Sokolov and Aranson 2009; Gachelin et al. 2013; López et al. 2015). However, we are not aware of prior experimental work indicating a negative contribution to the overall viscosity for oblate pullers, as is predicted here.

Figure 2 shows a schematic representation of the stresslet (force dipole exerted by the particle onto the fluid) for a prolate spheroid subject to a shear flow. The passive contribution to the stresslet, resulting from the imposed flow and Brownian rotation, always results in a compressional stresslet and therefore a positive contribution to the suspension viscosity. However, the active contribution, arising from the thrust force and compensating drag force generated from self-propulsion, can result in either a compressional or extensional stresslet, depending on the mechanism of self-propulsion. Prolate pullers, which generate thrust from the front, always have a compressional active stresslet, and therefore a compressional overall stresslet (Fig. 2a) and positive contribution to the suspension viscosity. Weak prolate pushers, which generate thrust from behind and are

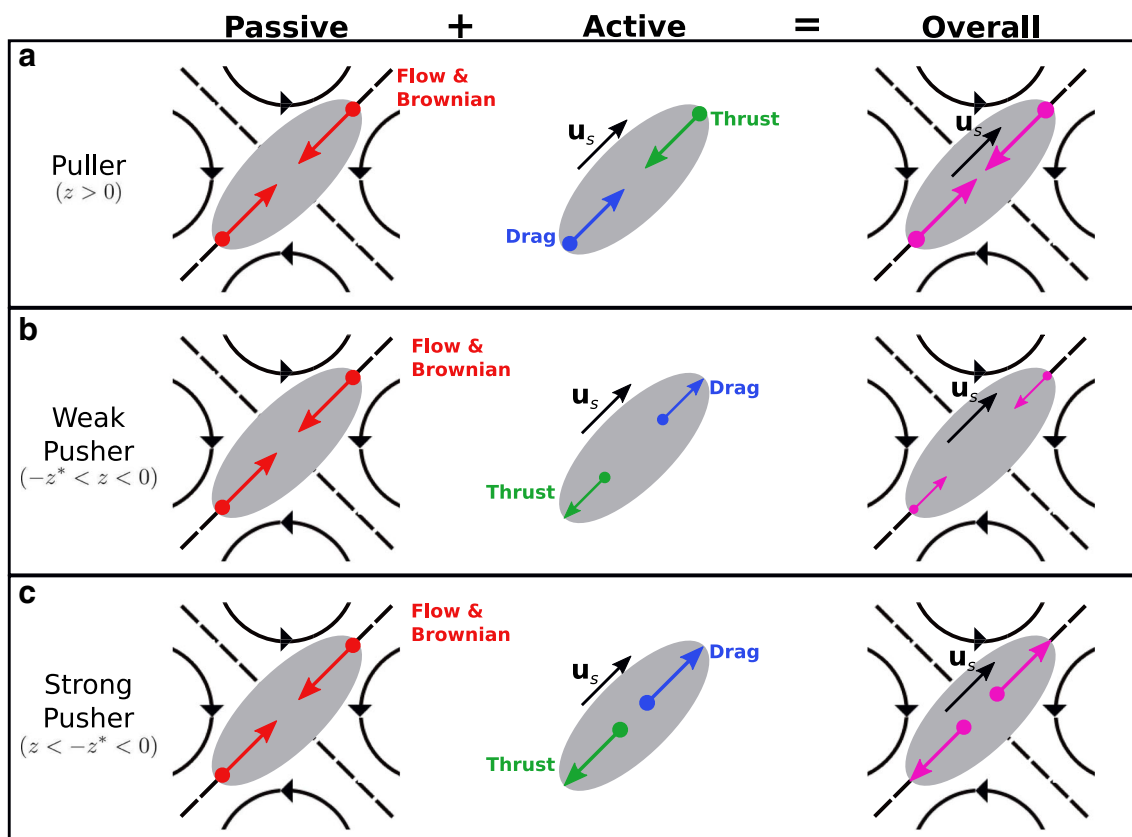


Fig. 2 Schematic of the stresslet for a prolate spheroid in steady shear flow for different self-propulsion mechanisms: **a** puller ($0 < z$), **b** weak pusher ($-z^* < z < 0$), and **c** strong pusher ($z < -z^* < 0$). The solid black lines represent the straining component of the flow and the dashed black lines the principle axes of strain. In the limit of $Wi \ll 1$, the flow, to leading order, acts to align the microstructure along the principle axes of strain. The passive contribution (left, red) to the stresslet, from the imposed flow and rotational Brownian motion,

always results in a compressional force dipole from the particle onto the fluid. However, the active contribution (middle, green, and blue) to the stresslet can be either compressional or extensional, depending on the mechanism of self-propulsion. Thus, for pullers and weak pushers, the overall stresslet (right, magenta) is compressional. Whereas, for strong pushers, the overall stresslet is extensional, resulting in a negative viscosity contribution. Here, u_s indicates the self-propelled swimming speed of particle

characterized by the dipole strength $-z^* < z < 0$, will have an extensional active stresslet, but a compressional overall stresslet (Fig. 2b). This results in a positive contribution to the suspension viscosity, but the magnitude of the viscosity increase is less than that of a passive suspension. Strong prolate pushers, characterized by $z < -z^* < 0$, will have an extensional active stresslet of greater magnitude than the passive stresslet contribution, resulting in an extensional overall stresslet (Fig. 2c) and a negative contribution to the suspension viscosity. Note that the overall viscosity of the suspension (η), which includes the contribution of the suspending medium (μ_s), will remain positive for a dilute suspension of prolate pullers or pushers, regardless of the magnitude of the dipole, as $\eta = \mu_s + c \eta^p$, where η^p is the particle contribution to the overall viscosity and $c (\ll 1)$ is the particle volume fraction

The linear relaxation modulus, $G_I(s)$, is defined as Macosko (1994),

$$G_I(s) = \frac{2}{\pi} \int_0^\infty \eta'(\alpha) \cos(\alpha s) ds, \tag{26}$$

and can be determined from Eq. 23 to be,

$$G_I(\tilde{t}) = \left(\frac{8A_H}{15} + \frac{4B_H}{3} + 2C_H \right) \delta(\tilde{t}) + \frac{B}{5} (2F_H \lambda + z) e^{-(1-J(\beta)+6\lambda)\tilde{t}}. \tag{27}$$

The linear relaxation modulus has the functional form of the Jeffrey’s model: an instantaneous response combined with stress relaxation via an exponentially fading memory, similar to that of passive spheroids (Abdel-Khalik et al. 1974; Bird et al. 1977; Bechtel and Khair 2017). In contrast to a suspension of passive spheroids, the rate of stress relaxation, $1/t_r$, which is defined from the argument of the exponential in Eq. 27, is

$$\frac{1}{t_r} = \frac{1}{t_T} + \frac{1}{t_B}, \tag{28}$$

where $t_T = \tau/[1 - J(\beta)]$ is the timescale of tumbling events and $t_B = 1/6D_r$ is the timescale of rotational Brownian motion. This combination of two stress relaxation mechanisms is analogous to a pair of resistors in parallel in an electrical circuit, where the overall resistance of the system (R_{total}) is the reciprocal of the sum of the reciprocal resistance of each resistor (R_i), $1/R_{total} = \sum_i 1/R_i$. Here, the overall rate of stress relaxation is the sum of the reciprocal of the timescale of each relaxation mechanism. The combination of stress relaxation from tumbling events and rotational Brownian motion increases the overall rate of stress relaxation, relative to a suspension of non-Brownian, active particles or a suspension of Brownian, inactive particles.

Figures 3 and 4 depict the complex viscosity of a dilute suspension of prolate ($r = 3$) and oblate ($r = 0.25$) spheroids, respectively, as a function of self-propulsion

Fig. 3 Viscous (η' , top) and elastic (η'' , bottom) components of the complex viscosity for a dilute suspension of active prolate spheroids ($r = 3$) for (1) a puller: $z = 50$, (2) a weak pusher: $z = -50$, and (3) a strong pusher: $z = -200$. Here, the ratio of tumbling frequency to rotational Brownian motion is varied: **a** $\lambda = 0$, **b** $\lambda = 0.1$, and **c** $\lambda = 1$ and $z^* = -150.4$, using $\lambda = 1$ and $\beta = 1$

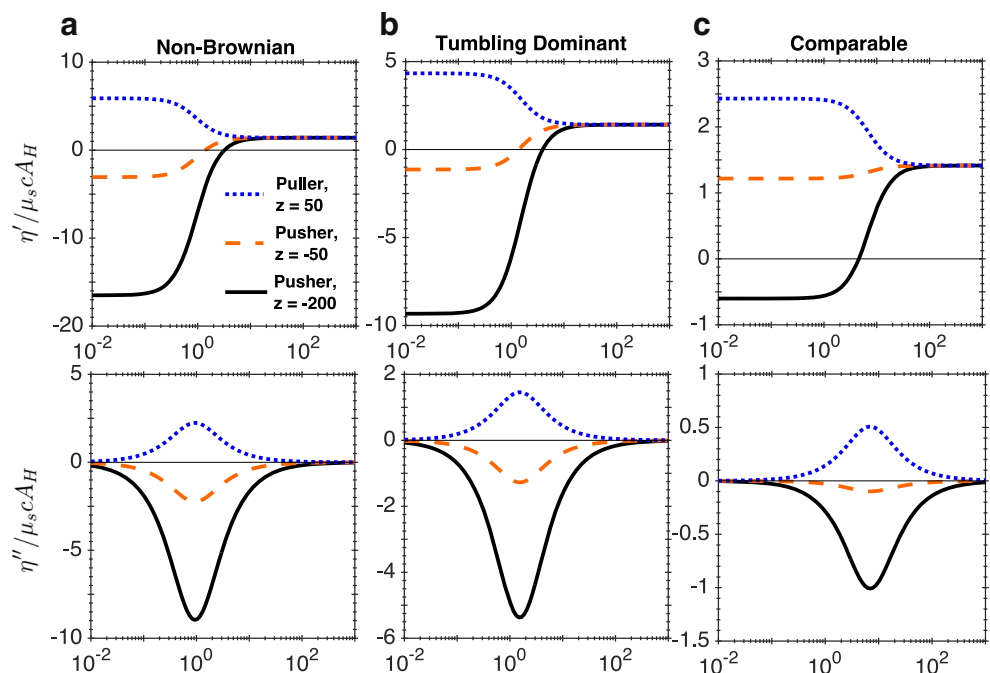
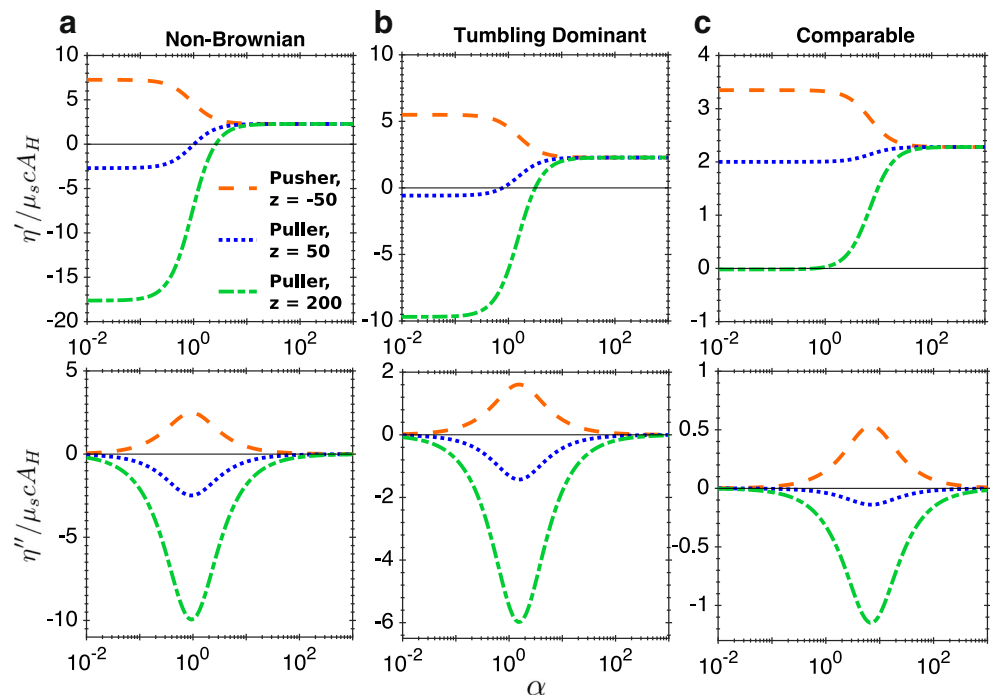


Fig. 4 Viscous (η' , top) and elastic (η'' , bottom) components of the complex viscosity for a dilute suspension of active oblate spheroids ($r = 0.25$) for (1) a pusher: $z = -50$, (2) a weak puller: $z = 50$, and (3) a strong puller: $z = 200$. Here, the ratio of tumbling frequency to rotational Brownian motion is varied: **a** $\lambda = 0$, **b** $\lambda = 0.1$, and **c** $\lambda = 1$ and $z^* = 198.5$, using $\lambda = 1$ and $\beta = 1$



mechanism, z , and relative importance of tumbling to rotational Brownian motion, λ . For both prolate and oblate spheroids, the plateau frequency, which is defined as the frequency at which the material response no longer changes, increases as the strength of rotational Brownian motion increases (i.e., as λ increases). Furthermore, we also observe that prolate pullers and oblate pushers will always have a positive viscous and elastic response, independent of frequency. Whereas, prolate pushers and oblate pullers with a dipole strength greater than the critical dipole strength, defined in Eq. 25, can have a negative viscous and elastic response at low frequency.

Comparison to previous work

Steady shear of active, slender rods ($r \rightarrow \infty$)

The particle contribution to the steady shear viscosity of a dilute suspension of active, slender rods ($r \rightarrow \infty$) was previously calculated by Saintillan (2010) for uncorrelated tumbling events ($\beta = 0$). We can compare these steady shear results to our linear viscoelastic response, via the Cox-Merz rule,

$$\eta(Wi) = |\eta^*|(\alpha), \quad (29)$$

which states that, for $Wi = \alpha$, the steady shear viscosity is equal to the magnitude of the frequency-dependent

complex viscosity. Figure 5 shows a comparison of the linear viscoelasticity and the steady shear viscosity for a puller and a pusher at $\lambda = 0.5$. In Fig. 5a, we observe that the Cox-Merz rule holds fairly well for prolate pullers, with a qualitative agreement overall all frequencies. For prolate pushers, which have a negative contribution to the overall viscosity of the suspension, the Cox-Merz rule does not hold, as the magnitude of the complex viscosity is always a positive quantity (Fig. 5b). However, we observe agreement between the steady shear viscosity and the viscous component of the complex viscosity up to $O(10)$ in the shear rate (Wi) or frequency (α). This indicates that the particle contribution to the steady shear viscosity is akin to the linear viscous response for an active suspension, up to moderate shear rate. That is, $\eta(\dot{\gamma}_0) = \eta'(\omega)$ is applicable beyond the zero-shear and zero-frequency limit and can be viewed as a modified Cox-Merz rule for active suspensions with a negative viscosity increment. The deviation between the steady shear and both the viscous complex viscosity and magnitude of the complex viscosity, at larger Wi and frequency, is consistent with passive colloidal systems (Al-Hadithi et al. 1992).

Experimental results for suspensions of *E. coli*

Now that we have demonstrated that a modified Cox-Merz rule is applicable to a dilute, active suspension, at least to moderate frequency and shear rate, we can extend our comparison to an experimental system. In Fig. 6, we

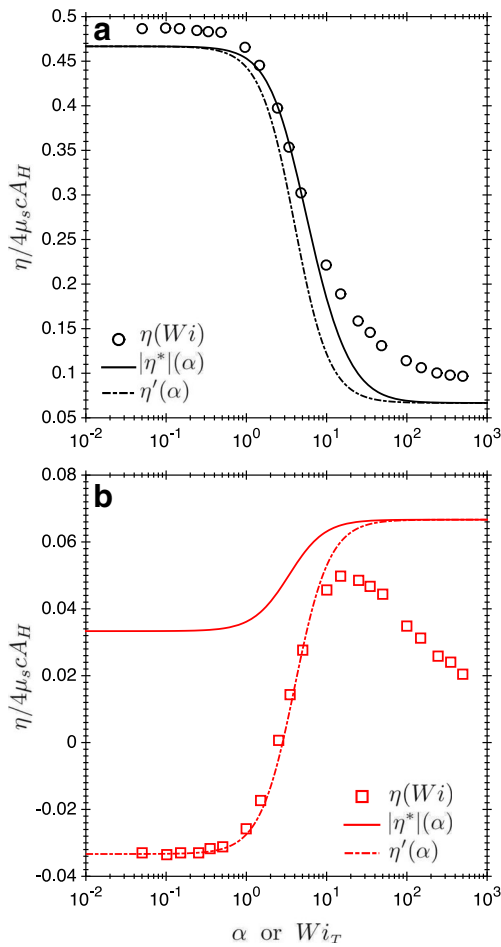


Fig. 5 Cox-Merz rule for active suspensions. Here, we compare our theoretical prediction to that of Saintillan (2010) (see his Fig. 5a) for $r \rightarrow \infty$, $\beta = 0$, $\lambda = 0.5$ (corresponding to $\bar{\tau} = 5$ and $\tilde{d}_r = 0.1$ in the notation of Saintillan (2010)) for **a** puller ($z = 4A_H$) and **b** pusher ($z = -4A_H$). The circles and squares are the digitized numerical results for the steady shear viscosity from Saintillan 2010. The solid line is the magnitude of the complex viscosity, from Eqs. 23–24, and the dot-dashed line is the viscous component of the complex viscosity, from Eq. 23

show the digitized steady shear viscosity measurements of López et al. (2015) for *E. coli* suspensions (symbols), which includes the contribution of the suspending medium, compared to the viscous component of the complex viscosity (23), at varied volume fractions (solid lines). The experimental parameters reported by López et al. (2015) utilized in Eq. 23 are $\tau^{-1} = 10$ Hz, $T = 298$ K, and $\mu_s = 1.4$ mPa. To determine the relative frequency of Brownian rotation to tumbling (λ), we first calculated the rotational diffusion coefficient for a single particle (Leal and Hinch 1971),

$$D_r = \frac{k_B T}{4\mu_s V_p} \left(\frac{r^2 K_3(r) + K_1(r)}{r^2 + 1} \right), \tag{30}$$

where,

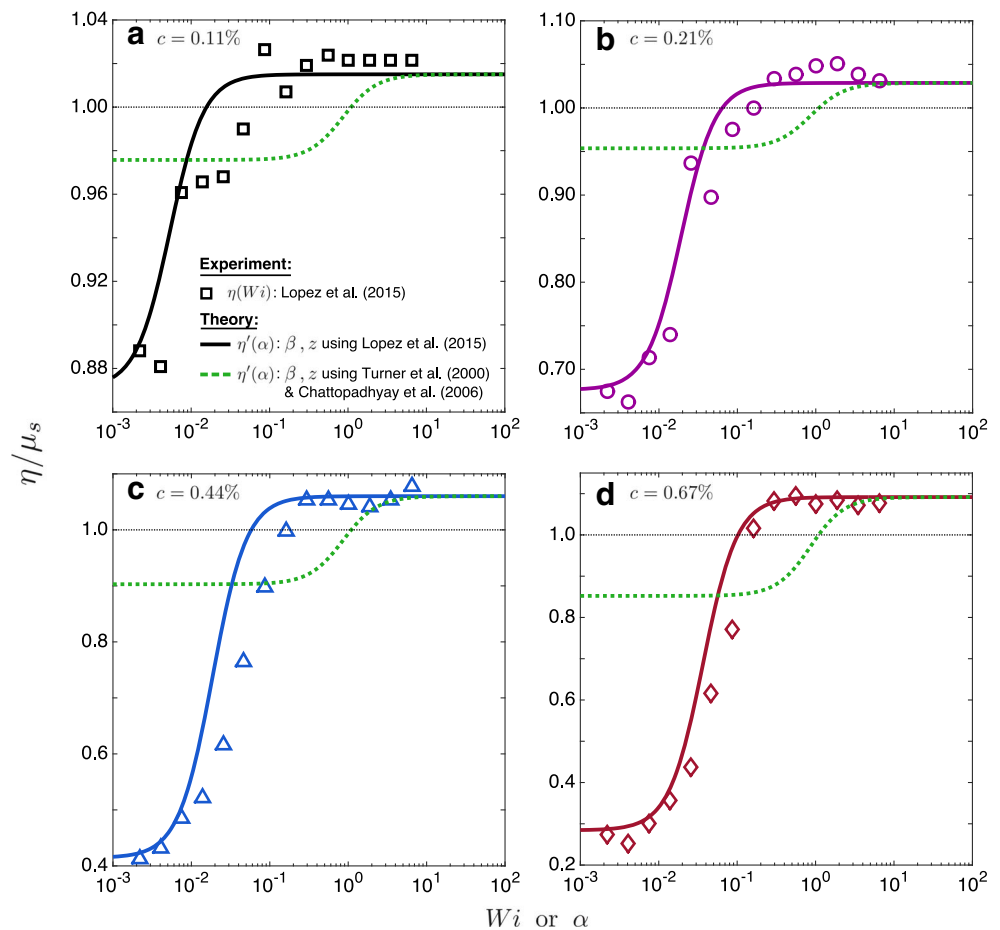
$$K_1(r) \equiv \int_0^\infty \frac{r ds}{(r^2 + s)^{1/2} (1 + s)^2}, \tag{31}$$

$$K_3(r) \equiv \int_0^\infty \frac{r ds}{(r^2 + s)^{3/2} (1 + s)}, \tag{32}$$

and k_B is the Boltzmann constant. Substitution of the given values for temperature and suspending medium viscosity, along with an estimate of aspect ratio of an *E. coli* cell, $r = 20$ ($\ell \sim 5 \mu\text{m}$ and $a \sim 0.25 \mu\text{m}$ (Trueba and Woldringh 1980; Gachelin et al. 2013; López et al. 2015)), into Eq. 30 yields $D_r = 0.009 \text{ s}^{-1}$. Thus, $\lambda = D_r/\tau^{-1} = 9 \times 10^{-4}$ and tumbling is the dominant mode of microstructural relaxation. Here, the estimate of the aspect ratio of an *E. coli* cell includes the length of the flagella tail that is responsible for self-propulsion and tumbling. Next, we utilized the steady shear viscosity measurements at $Wi = 0.002$ and $Wi = 0.007$ and the modified Cox-Merz rule via (23) to obtain a system of two equations and two unknowns (β and z); solving this system of equations simultaneously obtains β and z , which are listed for each volume fraction in Table 1. The dotted line in Fig. 6 is the viscous complex viscosity given in Eq. 23 for $\beta = 1.64$, corresponding to $\langle \theta \rangle = 58^\circ$ (Turner et al. 2000), and $z = -155.5$, corresponding to a thrust force, $F_{\text{thrust}} = \sigma_0/\ell = 0.57 \text{ pN}$ (Chattopadhyay et al. 2006).

From Fig. 6, we see a qualitative agreement between the steady shear viscosity measurements of López et al. (2015) and our prediction of the linear viscoelasticity, using the values of β and z in Table 1 at all values of Wi and α . However, the use of β obtained from fluorescence microscopy (Turner et al. 2000) and z from optical trapping of a single cell (Chattopadhyay et al. 2006) does not provide a reasonable agreement to the experimental data. This suggests that the measured self-propulsion characteristics of an active suspension are sensitive to the volume fraction of particles. Furthermore, the cell volume fractions utilized by López et al. (2015) are arguably beyond the dilute regime, where hydrodynamic interactions between cells is negligible; collective motion has been observed in suspensions of *E. coli* for $n = O(10^8)$ cells/mL (Wu et al. 2006), which corresponds to $c \sim 0.01\%$. Despite the fact that the data reported by López et al. (2015) is at volume fractions above this threshold, we surprisingly observe good agreement between their experimental results and our dilute theory. Thus, the

Fig. 6 Comparison of the linear viscoelasticity of a suspension of pushers to experimental measurements of the steady shear viscosity of *E. coli*, which include the contribution of the suspending medium, for cell volume fractions, c , of **a** 0.11%, **b** 0.21%, **c** 0.44%, and **d** 0.67%. The symbols are experimental data from López et al. (2015) (see their Fig. 1b) for $\mu_s = 1.4$ mPa, and $T = 298$. The solid line is the viscous complex viscosity in Eq. 23 using $r = 20$, $\tau = 0.1$ s, $\lambda = 9 \times 10^{-4}$, and the appropriate β and z values from Table 1. The volume fraction-dependent values of β and z were obtained from the steady shear viscosity measurements at $Wi = 0.002$ and $Wi = 0.007$. The dotted line is the viscous complex viscosity from Eq. 23, now using $\beta = 1.64$, which was obtained from fluorescence microscopy (Turner et al. 2000), and $z = -155.5$, which was obtained from optical trapping measurements (Chattopadhyay et al. 2006)



results from the SAOS of a dilute, active suspension are able to provide the self-propulsion characteristics of active particles; namely, the self-propulsion mechanism (pusher or puller), dipole strength ($|\sigma_0|$), and correlation between tumbling events (β).

Table 1 Volume fraction-dependent self-propulsion parameters of *E. coli*

| c | β | $\langle \theta \rangle$ | z | F_{thrust} (pN) |
|-------|----------|--------------------------|-------|--------------------------|
| 0.11% | ∞ | 0° | -4.2 | 0.015 |
| 0.21% | 223 | 4.8° | -16.9 | 0.062 |
| 0.44% | 233 | 4.7° | -14.5 | 0.053 |
| 0.67% | 96 | 7.3° | -22.9 | 0.084 |

The values of β and z were obtained by applying the modified Cox-Merz rule discussed in the “Steady shear of active, slender rods ($r \rightarrow \infty$)” section and equating the steady shear viscosity measurements of López et al. (2015) at $Wi = 0.002$ and 0.007 to the viscous component of the complex viscosity, given in Eq. 23, for $r = 20$, $\tau^{-1} = 10$ Hz, $\lambda = 9 \times 10^{-4}$, $\mu_s = 1.4$ mPa, and $T = 298$ K

Summary

We calculated the linear viscoelasticity of a dilute suspension of active spheroids of arbitrary aspect ratio subject to a SAOS deformation. The active suspension is characterized by two relaxation mechanisms: rotational Brownian motion and correlated tumbling. For weak deformation ($Wi \ll 1$), the particle contribution to the stress was determined from ensemble averages of the stresslets due to the imposed flow, rotational Brownian motion, and tumbling. From a comparison to the steady shear result of Saintillan (2010) for slender rods, we show that a modified Cox-Merz rule is applicable to a dilute active suspension. Furthermore, through a comparison with the experimental results of López et al. (2015) for *E. coli*, we demonstrated that from the SAOS of an active suspension, one can determine the mechanism of self-propulsion (pusher or puller) and estimate the strength of the dipole moment ($|\sigma_0|$) and correlation between tumbling events (β) of the particles. A natural extension to the present work would be to quantify how correlated tumbling affects the nonlinear rheology of an active

suspension, e.g., shear-thinning (or thickening) and normal stress coefficients.

Acknowledgments We thank Hriday Sattineni, a visiting undergraduate researcher from the Imperial College London, who verified our calculation for the uncorrelated tumbling regime ($\beta = 0$) and provided useful initial discussions. We acknowledge partial support from the Camille Dreyfus Teacher-Scholar Award program and the Department of Chemical Engineering at the Carnegie Mellon University.

Note added in proof After the present paper was accepted, a paper by S. Nambiar, P. R. Nott, and G. Subramanian (“Stress relaxation in a dilute bacterial suspension,” *J. Fluid Mech.* vol. 812, pp. 41–64) was published online on 22 December 2016. Their paper provides expressions for the storage (G') and loss (G'') moduli of a suspension of slender bacteria under weak oscillatory shear (see below equation (3.1) in their work). Those expressions can be recovered from the complex viscosity reported in (23) and (24) of the present work by: (i) using the definitions $G' = \omega\eta''$ and $G'' = \omega\eta'$; (ii) taking the limit of large aspect ratio, $r \rightarrow \infty$; (iii) neglecting Brownian stress; and (iv) assuming a dipole strength $\sigma_0 \sim \mu_s u_s l^2$, where u_s is the swimming speed of a bacterium.

References

- Abdel-Khalik SI, Hassager O, Bird RB (1974) The Goddard expansion and the kinetic theory for solutions of rodlike macromolecules. *J Chem Phys* 61(10):4312–4316. doi:10.1063/1.1681736
- Al-Hadithi TSR, Barnes HA, Walters K (1992) The relationship between the linear (oscillatory) and nonlinear (steady-state) flow properties of a series of polymer and colloidal systems. *Colloid Polym Sci* 270(1):40–46. doi:10.1007/BF00656927
- Bechtel TM, Khair AS (2017) Nonlinear relaxation modulus via dual-frequency medium amplitude oscillatory shear (maos): general framework and case study for a dilute suspension of Brownian spheroids. *J Rheology* 61(1):67–82
- Bird RB, Armstrong RC, Hassager O (1977) Dynamics of polymeric liquids. Volume 1: Fluid mechanics, edn. Wiley, New York
- Bozorgi Y, Underhill PT (2014) Large-amplitude oscillatory shear rheology of dilute active suspensions. *Rheologica Acta* 53(12):899–909. doi:10.1007/s00397-014-0806-y
- Brenner H, Condiff DW (1974) Transport mechanics in systems of orientable particles. IV. convective transport. *J Colloid Interface Sci* 47(1):199–264. doi:10.1016/0021-9797(74)90093-9
- Chapman S, Cowling T (1991) The mathematical theory of non-uniform gases. Cambridge University Press, Cambridge
- Chattopadhyay S, Moldovan R, Yeung C, Wu XL (2006) Swimming efficiency of bacterium *Escherichia coli*. *Proc Natl Acad Sci* 103(37):13,712–13,717. doi:10.1073/pnas.0602043103, arXiv:0512219
- Cox WP, Merz EH (1958) Correlation of dynamic and steady flow viscosities. *J Polym Sci* 28(118):619–622. doi:10.1002/pol.1958.1202811812
- Dey KK, Wong F, Altomose A, Sen A (2016) Catalytic motors—quo vadimus? *Curr Opin Colloid Interface Sci* 21:4–13. doi:10.1016/j.cocis.2015.12.001, <http://linkinghub.elsevier.com/retrieve/pii/S1359029415001120>
- Dhar P, Cao Y, Kline T, Pal P, Swayne C, Fischer TM, Miller B, Mallouk TE, Sen A, Johansen TH (2007) Autonomously moving local nanoprobe in heterogeneous magnetic fields. *J Phys Chem C* 111(9):3607–3613. doi:10.1021/jp067304d
- Ebbens SJ, Howse JR (2010) In pursuit of propulsion at the nanoscale. *Soft Matter* 6(4):726. doi:10.1039/b918598d
- Gachelin J, Miño G, Berthet H, Lindner A, Rousselet A, Clément É (2013) Non-Newtonian viscosity of *Escherichia coli* Suspensions. *Phys Rev Lett* 110(26):268,103. doi:10.1103/PhysRevLett.110.268103
- Haines BM, Aronson IS, Berlyand L, Karpeev DA (2008) Effective viscosity of dilute bacterial suspensions: a two-dimensional model. *Phys Biol* 5(4):046,003. doi:10.1088/1478-3975/5/4/046003, <http://stacks.iop.org/1478-3975/5/i=4/a=046003?key=crossref.dd72c17be44d02d6e72f1d394e6cd465>
- Hatwalne Y, Ramaswamy S, Rao M, Simha RA (2004) Rheology of active-particle suspensions. *Phys Rev Lett* 92(11):118,101. doi:10.1103/PhysRevLett.92.118101
- Hinch EJ, Leal LG (1972) The effect of Brownian motion on the rheological properties of a suspension of non-spherical particles. *J Fluid Mech* 52(4):683–712
- Hinch EJ, Leal LG (1976) Constitutive equations in suspension mechanics. Part 2. Approximate forms for a suspension of rigid particles affected by Brownian rotations. *J Fluid Mech* 76(01):187–208. doi:10.1017/S0022112076003200
- Hong Y, Velegol D, Chaturvedi N, Sen A (2010) Biomimetic behavior of synthetic particles: from microscopic randomness to macroscopic control. *Phys Chem Chem Phys* 12(7):1423–1435. doi:10.1039/B917741H
- Jeffery G (1922) The motion of ellipsoidal particles immersed in a viscous fluid. *Proc Roy Soc Lond A* 102(715):161–179
- Kim S, Karrila SJ (2005) Microhydrodynamics: principles and selected applications. Dover Mineola, New York
- Kline TR, Paxton WF, Mallouk TE, Sen A (2005) Catalytic nanomotors: remote-controlled autonomous movement of striped metallic nanorods. *Angewandte Chemie* 117(5):754–756. doi:10.1002/ange.200461890
- Lauga E, Powers TR (2009) The hydrodynamics of swimming microorganisms. *Rep Prog Phys* 72(9):096,601. doi:10.1088/0034-4885/72/9/096601, <http://stacks.iop.org/0034-4885/72/i=9/a=096601?key=crossref.736a5c13368e75b7395f94099aead8e4>
- Leal LG, Hinch EJ (1971) The effect of weak Brownian rotations on particles in shear flow. *J Fluid Mech* 46(4):685–703. doi:10.1017/S0022112071000788
- López HM, Gachelin J, Douarche C, Auradou H, Clément E (2015) Turning bacteria suspensions into superfluids. *Phys Rev Lett* 115(2):028,301. doi:10.1103/PhysRevLett.115.028301
- Macosko CW (1994) Rheology: principles, measurements and applications. Wiley-VCH, New York
- McQuarrie DA (2000) Statistical mechanics. University Science Books
- Mussler M, Rafai S, Peyla P, Wagner C (2013) Effective viscosity of non-gravitactic *Chlamydomonas Reinhardtii* microswimmer suspensions. *Europhys Lett* 101(5):54,004. doi:10.1209/0295-5075/101/54004, arXiv:1310.1482
- Patra D, Sengupta S, Duan W, Zhang H, Pavlick R, Sen A (2013) Intelligent, self-powered, drug delivery systems. *Nanoscale* 5(4):1273–1283. doi:10.1039/C2NR32600K
- Rafai S, Jibuti L, Peyla P (2010) Effective viscosity of microswimmer suspensions. *Phys Rev Lett* 104(9):098,102. doi:10.1103/PhysRevLett.104.098102
- Saintillan D (2010) The dilute rheology of swimming suspensions: a simple kinetic model. *Exp Mech* 50(9):1275–1281. doi:10.1007/s11340-009-9267-0
- Saintillan D, Shelley MJ (2008) Instabilities, pattern formation, and mixing in active suspensions. *Phys Fluids* 20(12):123,304. doi:10.1063/1.3041776
- Schwarz-Linek J, Arlt J, Jepsen A, Dawson A, Vissers T, Mioli D, Pilizota T, Martinez VA, Poon WC (2016) *Escherichia coli* as a model active colloid: a practical introduction. *Colloids Surf B Biointerfaces* 137:2–16. doi:10.1016/j.colsurfb.2015.07.048, <http://linkinghub.elsevier.com/retrieve/pii/S0927776515300825>

- Sokolov A, Aranson IS (2009) Reduction of viscosity in suspension of swimming bacteria. *Phys Rev Lett* 103(14):148,101. doi:[10.1103/PhysRevLett.103.148101](https://doi.org/10.1103/PhysRevLett.103.148101)
- Spagnolie SE (2015) Complex fluids in biological systems. *Biological and Medical Physics, Biomedical Engineering*. Springer, New York. doi:[10.1007/978-1-4939-2065-5](https://doi.org/10.1007/978-1-4939-2065-5)
- Stenhammar J, Marenduzzo D, Allen RJ, Cates ME (2014) Phase behaviour of active Brownian particles: the role of dimensionality. *Soft Matter* 10(10):1489–1499. doi:[10.1039/C3SM52813H](https://doi.org/10.1039/C3SM52813H)
- Subramanian G, Koch DL (2009) Critical bacterial concentration for the onset of collective swimming. *Journal of Fluid Mechanics* 632:359. doi:[10.1017/S002211200900706X](https://doi.org/10.1017/S002211200900706X)
- Sundararajan S, Lammert PE, Zudans AW, Crespi VH, Sen A (2008) Catalytic motors for transport of colloidal cargo. *Nano Lett* 8(5):1271–1276. doi:[10.1021/nl072275j](https://doi.org/10.1021/nl072275j)
- Takatori SC, Yan W, Brady JF (2014) Swim pressure: stress generation in active matter. *Phys Rev Lett* 113(2):028,103. doi:[10.1103/PhysRevLett.113.028103](https://doi.org/10.1103/PhysRevLett.113.028103)
- Teo WZ, Pumera M (2016) Motion control of micro-/nanomotors. *Chemistry—A European Journal* pp 1–10. doi: [10.1002/chem.201602241](https://doi.org/10.1002/chem.201602241)
- Tjhung E, Cates ME, Marenduzzo D (2011) Nonequilibrium steady states in polar active fluids. *Soft Matter* 7(16):7453. doi:[10.1039/c1sm05396e](https://doi.org/10.1039/c1sm05396e)
- Trueba FJ, Woldringh CL (1980) Changes in cell diameter during the division cycle of *Escherichia coli*. *J Bacteriol* 142(3):869–78. <http://www.ncbi.nlm.nih.gov/pubmed/6769914>, <http://www.pubmedcentral.nih.gov/articlerender.fcgi?artid=PMC294112>
- Turner L, Ryu WS, Berg HC (2000) Real-time imaging of fluorescent flagellar filaments. *J Bacteriol* 182(10):2793–2801. doi:[10.1128/JB.182.10.2793-2801.2000](https://doi.org/10.1128/JB.182.10.2793-2801.2000)
- Wu M, Roberts JW, Kim S, Koch DL, DeLisa MP (2006) Collective bacterial dynamics revealed using a three-dimensional population-scale defocused particle tracking technique. *Appl Environ Microbiol* 72(7):4987–4994. doi:[10.1128/AEM.00158-06](https://doi.org/10.1128/AEM.00158-06)